GENERALIZED CRITERIA FOR DYNAMIC INSTABILITY

By Warren L. Godson

Meteorological Service of Canada[1]

(Original manuscript received 20 November 1947; revised manuscript received 20 January 1950)

ABSTRACT

The "parcel" method of treating dynamic instability is extended to the case of an arbitrary flow pattern. The criteria for instability become relatively complex and depend on the three-dimensional gradients of temperature and geostrophic wind, as well as on the latitude. Fundamentally different types of instability and stability may arise; these are illustrated by typical examples. Methods for the computation of the various terms in the fundamental stability-criterion parameters are presented, and these methods, as well as the generalized criteria themselves, are extended to the case of saturated air.

It is suggested that marked quasi-horizontal, or dynamic, instability will superimpose a strong field of "perturbation divergence" on the ambient field of mass divergence and hence should be a significant factor in the weakening of anticyclones and the formation and deepening of cyclones.

1. Introduction

Weather forecasting usually requires estimation of the motion and development of pressure areas and frontal systems. In many cases, developments could be adequately forecast, in theory at least, by straightforward application of the hydrodynamical equations of motion and continuity, the equation of state, the laws of thermodynamics, and the equations of eddy and radiative transfer. Other developments appear to arise as a result of small perturbations which, if unstable, can exert a trigger action on the atmospheric state and thereby cause large-scale developments, quite unpredictable on a rigorous, classical basis.

It is obviously important to be able to assess the probability of occurrence of such developments, arising from instability. There are two methods available: the perturbed-wave method and the perturbed-parcel method. In the perturbed-wave method, an initial relatively simple, steady state of the atmosphere is assumed, such as zonal flow, and the possibility of the development of waves of small amplitude is investigated. When this is done, it is found that the long waves in the westerlies are an essential dynamic feature of the general circulation; pure zonal flow, when observed, is almost invariably unstable, and meridional circulations are soon established. Due to the restrictions which must be placed on the initial atmospheric state, it is not possible to apply the perturbed-wave treatment to a normal, well-developed sinusoidal flow, especially if asymmetries exist with regard to pressure and/or temperature. In other words, an entirely new tool is required, one which will predict the physical consequences of perturbed motion for an atmosphere which is far from homogeneous or symmetrical, an atmosphere in which space and time changes of the fundamental variables exist, defying a wave-perturbation treatment. The perturbed-parcel concept has proven invaluable in the prediction of the consequences of vertical or static instability, and there is good reason to believe it will also prove invaluable in assessing the results of the release of quasi-horizontal or dynamic instability.

In recent years, numerous studies have established that a statically stable atmosphere may, under certain circumstances, be unstable for quasi-horizontal perturbations. Previous investigations (see, for example, Solberg, 1936; Kleinschmidt, 1941; Van Mieghem, 1946, 1947) have applied only to rather restricted atmospheric models. The present paper presents the derivation of generalized criteria for dynamic instability, applicable to any given flow pattern and thermal field. A later paper[2] discusses the physical significance of dynamic instability and presents synoptic and statistical results of tests of this concept.

2. Equation of motion for a displaced air parcel

Consider the motions of an air parcel which is given an impulse, and a moving air parcel of the environment which has not been perturbed. Let $\boldsymbol{R}$ represent the position vector of the non-perturbed parcel (point N) and $\boldsymbol{r}$ the position vector of the perturbed parcel (point P). Let ρ and ρ_E denote the density of the perturbed parcel and of the environment, respectively. Let $(\rho_E^{-1}\nabla p)_N$ denote the pressure-gradient force on the non-perturbed parcel, and let $(\rho_E^{-1}\nabla p)_P$ denote the pressure-gradient force on the environment of the perturbed parcel. Let g represent the acceleration of gravity, $\boldsymbol{k}$ the vertical unit vector, and $\boldsymbol{\Omega}$ the earth's angular velocity.

[1] Published by permission of the Controller, Meteorological Division, Department of Transport.

[2] *Ed. note:* See next issue of the JOURNAL, Vol. 7, No. 5, October, 1950.

The equation of motion of the non-perturbed parcel is

$$d^2\boldsymbol{R}/dt^2 + 2\boldsymbol{\Omega} \times d\boldsymbol{R}/dt = -(\rho_E^{-1}\nabla p)_N - g\boldsymbol{k}. \quad (1)$$

The equation of motion of the perturbed parcel is

$$d^2\boldsymbol{r}/dt^2 + 2\boldsymbol{\Omega} \times d\boldsymbol{r}/dt = -\rho^{-1}\rho_E(\rho_E^{-1}\nabla p)_P - g\boldsymbol{k}. \quad (2)$$

Since the pressure on the perturbed parcel and on its environment are the same, it follows that

$$\rho_E\theta_E = \rho\theta. \quad (3)$$

Here θ_E represents the potential temperature of the environment at P, and θ the potential temperature of the perturbed parcel. It may be assumed that only adiabatic processes take place and that, prior to the perturbation impulse, the two air parcels considered were contiguous. Thus, θ also represents the potential temperature of the environment at N, the position occupied by the non-perturbed parcel. If $\boldsymbol{R}$ and $\boldsymbol{r}$ are small quantities, application of Taylor's theorem yields

$$\theta = \theta_E + (\boldsymbol{R} - \boldsymbol{r})\cdot\nabla\theta_E.$$

Denote the position vector of the perturbed parcel relative to the non-perturbed parcel by $\boldsymbol{r}'$. Then

$$\theta = \theta_E - \boldsymbol{r}'\cdot\nabla\theta_E. \quad (4)$$

Thus,

$$\rho^{-1}\rho_E = 1 - \theta_E^{-1}\boldsymbol{r}'\cdot\nabla\theta_E = 1 - \boldsymbol{r}'\cdot\nabla(\ln\theta_E). \quad (5)$$

Analogous to (4),

$$(\rho_E^{-1}\nabla p)_P = (\rho_E^{-1}\nabla p)_N + \boldsymbol{r}'\cdot\nabla(\rho_E^{-1}\nabla p). \quad (6)$$

Introduction of (5) and (6) into (2) and neglect of the squared terms in the relative displacement vector leads to

$$d^2\boldsymbol{r}/dt^2 + 2\boldsymbol{\Omega} \times d\boldsymbol{r}/dt = (\rho_E^{-1}\nabla p)_N\,\boldsymbol{r}'\cdot\nabla(\ln\theta_E) - \boldsymbol{r}'\cdot\nabla(\rho_E^{-1}\nabla p) - (\rho_E^{-1}\nabla p)_N - g\boldsymbol{k}. \quad (7)$$

If (1) is subtracted from (7) and subscripts denoting the environment are dropped,

$$d^2\boldsymbol{r}'/dt^2 + 2\boldsymbol{\Omega} \times d\boldsymbol{r}'/dt = (\rho^{-1}\nabla p)\,\boldsymbol{r}'\cdot\nabla(\ln\theta) - \boldsymbol{r}'\cdot\nabla(\rho^{-1}\nabla p). \quad (8)$$

This is the differential equation describing the motion of a perturbed parcel relative to the motion of a non-perturbed parcel.

3. Solutions of equation of relative motion

To solve (8), it is necessary to express the equation in component form. Refer the motion to a set of right-handed Cartesian axes with x and y horizontal (and orthogonal), but otherwise arbitrary, and z vertical. Let the corresponding components of $\boldsymbol{r}'$ be x', y', and z'. Set $\lambda = 2\bar{\omega}\sin\phi$, $\mu = 2\bar{\omega}\cos\phi\sin\psi$, and $\nu = 2\bar{\omega}\cos\phi\cos\psi$, where $\bar{\omega}$ represents the angular speed of rotation of the earth, ϕ the latitude, and ψ the angle from the east direction to the x-axis. Set $\rho^{-1}\,\partial p/\partial x = \lambda v_g$ and $\rho^{-1}\,\partial p/\partial y = -\lambda u_g$, where u_g and v_g represent the x- and y-components of the geostrophic wind. Set $\rho^{-1}\,\partial p/\partial z = -g$, since this is assumed in computations of pressure-height data and is an extremely good approximation for the environment.

To eliminate from consideration perturbations associated with long waves, it suffices to consider λ, μ, and ν as independent of x and y. The results will thus apply to those atmospheric domains in which variations of u_g and v_g with x and y are relatively greater than those of λ, μ, and ν.

With the introduction of dot superscripts to denote time differentiation following an air parcel, it follows that the component equations of (8) are

$$\ddot{x}' + \nu\dot{z}' - \lambda\dot{y}' = \lambda\left[v_g\frac{\partial(\ln\theta)}{\partial x} - \frac{\partial v_g}{\partial x}\right]x' + \lambda\left[v_g\frac{\partial(\ln\theta)}{\partial y} - \frac{\partial v_g}{\partial y}\right]y' + \lambda\left[v_g\frac{\partial(\ln\theta)}{\partial z} - \frac{\partial v_g}{\partial z}\right]z', \quad (9)$$

$$\ddot{y}' + \lambda\dot{x}' - \mu\dot{z}' = -\lambda\left[u_g\frac{\partial(\ln\theta)}{\partial x} - \frac{\partial u_g}{\partial x}\right]x' - \lambda\left[u_g\frac{\partial(\ln\theta)}{\partial y} - \frac{\partial u_g}{\partial y}\right]y' - \lambda\left[u_g\frac{\partial(\ln\theta)}{\partial z} - \frac{\partial u_g}{\partial z}\right]z', \quad (10)$$

and

$$\ddot{z}' + \mu\dot{y}' - \nu\dot{x}' = -g\frac{\partial(\ln\theta)}{\partial x}x' - g\frac{\partial(\ln\theta)}{\partial y}y' - g\frac{\partial(\ln\theta)}{\partial z}z'. \quad (11)$$

To the approximation afforded by the first order Taylor expansions, the coefficients of x', y', and z' may be considered as constants. The above three equations of relative motion thus represent a set of simultaneous, linear, homogeneous differential equations with constant coefficients and may be solved by standard methods (Ford, 1933).

It is known that solutions of (9)–(11) for x', y', and z', will be of the form $\exp[\pm i\omega t]$, where $i = (-1)^{\frac{1}{2}}$ and ω, the frequency of the oscillations, may be real, complex, or pure imaginary. Substitution of such solutions in (9)–(11) (*i.e.*, $A\cos\omega t + B\sin\omega t$ for x', *etc.*) eventually yields a cubic equation in ω^2 which permits of no simple solution. It is obvious that the problem would be greatly simplified if a close approximation to one solution for ω^2 could be obtained.

One fundamental frequency for the oscillation of perturbed parcels in the atmosphere is already known:

the familiar gravity-stability frequency of a static atmosphere for oscillations perpendicular to isentropic surfaces. It is also known that the removal of the static restriction has very little effect on the frequency itself.

By a consideration of order of magnitudes of the various terms involved, it may be demonstrated that one solution to the set is

$$x' = z'[-(dz/dx)_\theta \pm 10^{-4}], \tag{12}$$

$$y' = z'[-(dz/dy)_\theta \pm 10^{-4}], \tag{13}$$

$$z' = A\cos\omega t + B\sin\omega t, \tag{14}$$

$$\omega = [g\,\partial(\ln\theta)/\partial z]^{\frac{1}{2}}[1 \pm 10^{-4}]. \tag{15}$$

Thus, to a high degree of precision, except in the trivial case of neutral static equilibrium, one solution of the perturbation equations corresponds to the conventional gravity oscillations, with periods of the order of 10 min.

From a consideration of the symmetry properties of the original differential equations, it may be deduced directly that the remaining two modes of vibration represent relative oscillations in isentropic surfaces, or at least very nearly so. The general solution of the differential equations thus consists of the combination, with arbitrary coefficients, of two solutions: one normal to isentropic surfaces and one parallel to isentropic surfaces. The two modes of vibration in the latter solution cannot occur independently, as will be seen later, because of the condition that $x' = y' = z'$ at $t = 0$.

4. Solutions for isentropic component of relative motion

For the isentropic component of the relative motion,

$$z' = x'(dz/dx)_\theta + y'(dz/dy)_\theta. \tag{16}$$

As a result, the terms $\nu\dot{z}'$ and $\mu\dot{z}'$ in (9) and (10) are considerably smaller than the remaining Coriolis terms, and may be neglected. Substitution of (16) in (9) and (10) thus leads to

$$\ddot{x}' - \lambda\dot{y}' = -\lambda x'(\partial v_g/\partial x)_\theta - \lambda y'(\partial v_g/\partial y)_\theta, \tag{17}$$

$$\ddot{y}' + \lambda\dot{x}' = \lambda x'(\partial u_g/\partial x)_\theta + \lambda y'(\partial u_g/\partial y)_\theta. \tag{18}$$

The solutions of (17) and (18) can be obtained by setting

$$x' = A\cos\omega t + B\sin\omega t, \tag{19}$$

$$y' = C\cos\omega t + D\sin\omega t. \tag{20}$$

Substitution of (19) and (20) in (17) and (18) yields four equations in A, B, C, and D. For non-zero solutions, it is necessary that the determinant of the coefficients of A, B, C, and D vanish identically. The evaluation of this determinant equation results in a binomial equation in ω^2. This equation may be expressed in a condensed form by the following symbolic substitutions:

$$\begin{aligned}(\partial u_g/\partial x)_\theta &= M_x, \qquad (\partial u_g/\partial y)_\theta = M_y,\\ (\partial v_g/\partial x)_\theta &= N_x, \qquad (\partial v_g/\partial y)_\theta = -M_x.\end{aligned} \tag{21}$$

The validity of the last substitution in (21) may be established simply and, indeed, follows at once from the fact that an isentropic stream function for the geostrophic wind can be derived. Using (21), the frequency equation becomes

$$\omega^4 + \omega^2\lambda(M_y - N_x - \lambda) - \lambda^2(M_x^2 + M_yN_x) = 0. \tag{22}$$

It is advantageous to express (22) in a non-dimensional form,

$$(\omega/\lambda)^4 - b(\omega/\lambda)^2 + c = 0, \tag{23}$$

where

$$b = 1 + \lambda^{-1}(N_x - M_y), \tag{24}$$

and

$$c = -\lambda^{-2}(M_x^2 + M_yN_x). \tag{25}$$

The solution of (23) is

$$(\omega/\lambda)^2 = \tfrac{1}{2}b \pm [\tfrac{1}{4}b^2 - c]^{\frac{1}{2}}. \tag{26}$$

Since the tentative solutions were of the form $\exp[\pm i\omega t]$, (26) defines two roots for ω, whose nature will depend on the values of b and c. Various cases are possible.

1. $c > \frac{1}{4}b^2$. In this case the roots of (26) for ω^2 are complex conjugates, and the corresponding values for ω are complex. The relative displacement components thus contain real exponential functions, and a stable oscillation is not possible, *i.e.*, dynamic instability is present. On the fundamental "b–c diagram," or instability-criterion diagram, of fig. 1 this domain is labelled as zone B. The dashed curve on that diagram has the equation $c - \frac{1}{4}b^2 = 0$.

2. $0 < c < \frac{1}{4}b^2$. In this case the sign of $(\omega/\lambda)^2$ is that of b, so that two different cases arise.

2a. $0 < c < \frac{1}{4}b^2$, $b > 0$. Here both roots for ω are real quantities, and a stable oscillation results. This domain is labelled as zone A on fig. 1.

2b. $0 < c < \frac{1}{4}b^2$, $b < 0$. Here both roots for ω are pure imaginary quantities. The relative displacement components thus consist entirely of real exponential

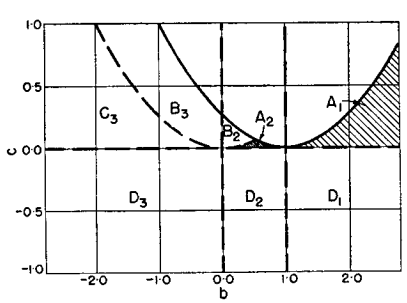

FIG. 1. Stability parameter diagram and zones of instability.

functions, and stable oscillations are not possible. This corresponds to a dynamically unstable state of the atmosphere for all initial isentropic impulses and is represented on fig. 1 as zone C.

3. $c < 0$. In this case one root of ω is real and the other pure imaginary. Except for a single trivial case, the initial conditions can be satisfied only if increasing exponential functions of time appear in the expressions for the relative displacement components. Hence, dynamic instability is present for this domain, denoted by zone D on fig. 1.

It may be deduced from (24) and (25) that, for a given value of b, there exists a certain maximum of c which is

$$c_m = \tfrac{1}{4}(b - 1)^2. \tag{27}$$

The solid curve in fig. 1, which has the above equation, blocks off those values of c which are not possible. The zones in fig. 1 are further subdivided according to whether $b > 1$ (sub-zone 1), $0 < b < 1$ (sub-zone 2), or $b < 0$ (sub-zone 3). The significance of this classification will appear later.

In fig. 1, the zone of dynamic stability (A) is indicated by hatching. For all other zones (B, C, and D), either complex or imaginary roots exist, and, hence, dynamic instability is present. Although no *single* criterion can be advanced which will differentiate zone A from the remaining zones, one condition can be presented which is of interest in the light of the historical development of the subject. Since c must be positive in zone A, it is evident from (25) that M_y and N_x must have opposite signs. Since b must also be positive in zone A, it follows from (24) that $(\lambda - M_y)$ must be positive, as well as $(\lambda + N_x)$. Thus $\lambda > (\partial u_g/\partial y)_\theta$ is a *necessary but not a sufficient condition* for dynamic stability. Earlier investigations with simple models (assuming $v_g \equiv 0$ and a steady state) had suggested that this inequality was both a necessary and a sufficient condition for dynamic stability.

The preceding analysis has established the general nature of the solutions of the perturbation equations and has delineated those domains on a parametric diagram associated with non-real frequencies and, hence, with dynamic instability. Further considerations, such as estimation of the degree of instability as a function of the direction of the initial impulse for the separate zones, will be discussed in the following sections.

5. Perturbed motion in zone of real frequencies

In zone A, the roots of the frequency equation, ω_1 and ω_2, are real and are defined by (26). The solutions for the perturbation components, x', y', and z', can be obtained if the initial conditions are introduced. In terms of Υ, the relative velocity vector $(\dot{r}')$, the initial conditions (at $t = 0$) are

$$x' = y' = 0, \qquad \dot{x}' = \Upsilon_{0x}, \qquad \dot{y}' = \Upsilon_{0y}.$$

z' and its derivatives are specified by x' and y' and their derivatives, for the isentropic relative-motion component. It may be demonstrated that the solutions for x' and y' in zone A are

$$x' = A(\cos \omega_1 t - \cos \omega_2 t) + B_1 \sin \omega_1 t + B_2 \sin \omega_2 t, \tag{28}$$

$$y' = C(\cos \omega_1 t - \cos \omega_2 t) + D_1 \sin \omega_1 t + D_2 \sin \omega_2 t, \tag{29}$$

$$A(\omega_1^2 - \omega_2^2) = -\lambda \Upsilon_{0y}. \tag{30}$$

$$C(\omega_1^2 - \omega_2^2) = \lambda \Upsilon_{0x}, \tag{31}$$

$$\lambda\omega B = \lambda M_x A + (\lambda M_y + \omega^2)C, \tag{32}$$

$$\lambda\omega D = (\lambda N_x - \omega^2)A - \lambda M_x C. \tag{33}$$

B_1, for example, is obtained from (32), using ω_1, A, and C; B_2 by using ω_2, $-A$, and $-C$, *etc.*

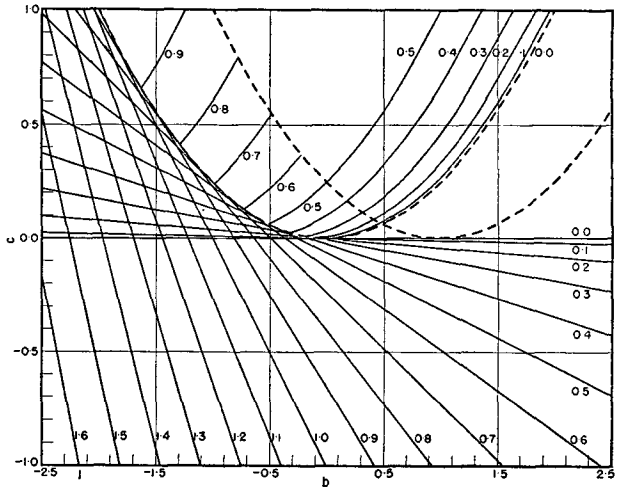

FIG. 2. Frequency diagram (isopleths of α/λ).

The ratios (ω/λ) can conveniently be found graphically, using the frequency diagram, fig. 2. The lines on this diagram are for values of (α/λ), where α is the exponential parameter for non-real frequencies, *i.e.*, $\alpha^2 = -\omega^2$. From (26), it is evident that ω_1 and ω_2 in zone A can be found from α_1 and α_2 in zone C, replacing b by $-b$.

The perturbed motion, here of the stable type, will depend on the orientation of the initial impulse [arc tan $(-A/C)$], when all other factors are kept constant. The best criterion of the degree of dynamic stability is simply the root-mean-square displacement $(\overline{r^2})^{\frac{1}{2}}$ of the perturbed parcel relative to the unperturbed parcel, using, for simplicity, r^2 for $(x'^2 + y'^2)$. This quantity may also be termed the effective amplitude of the relative motion. $\overline{r^2}$ may be obtained by integrating r^2 over a sufficiently long time interval to

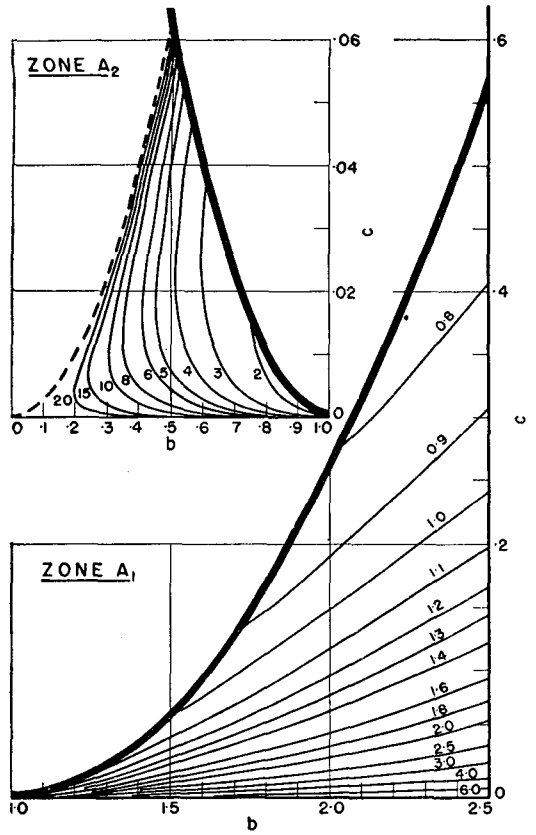

FIG. 3. Effective-amplitude factor for stable oscillations.

reproduce the initial conditions. Maximum and minimum effective amplitudes can then be investigated for a fixed initial impulse velocity Υ_0. These amplitudes have initial orientations given by

$$\frac{\Upsilon_{0_y}}{\Upsilon_{0_x}} = \frac{M_y + N_x}{2M_x} \pm \left[\left(\frac{M_y + N_x}{2M_x}\right)^2 + 1\right]^{\frac{1}{2}}. \quad (34)$$

It may further be shown that the mean value of $\overline{r^2}$ for any two initially-orthogonal relative trajectories is the same as for the set defined by (34). Thus, the mean of the maximum and minimum of $\overline{r^2}$ represents also the mean value, $\overline{\overline{r^2}}$ (over time and space), for all possible trajectories, assuming equal probabilities. The mean effective amplitude $(\overline{\overline{r^2}})^{\frac{1}{2}}$ has the value

$$(\overline{\overline{r^2}})^{\frac{1}{2}} = \left[\frac{2 - b + b(1 - b)^2/4c}{b^2 - 4c}\right]^{\frac{1}{2}} \frac{\Upsilon_0}{\lambda}. \quad (35)$$

The square-root expression on the right is plotted in fig. 3 for zones A_1 and A_2, separately. When divided by the Coriolis parameter (in hr^{-1}), it gives that fraction of the initial perturbation velocity (in miles hr^{-1}) which represents the mean effective amplitude of the relative trajectory (in miles). This fraction is thus a measure of the intensity of isentropic (and hence of quasi-horizontal) mixing processes. It will be observed that zone A_2 is in general considerably less stable than zone A_1.

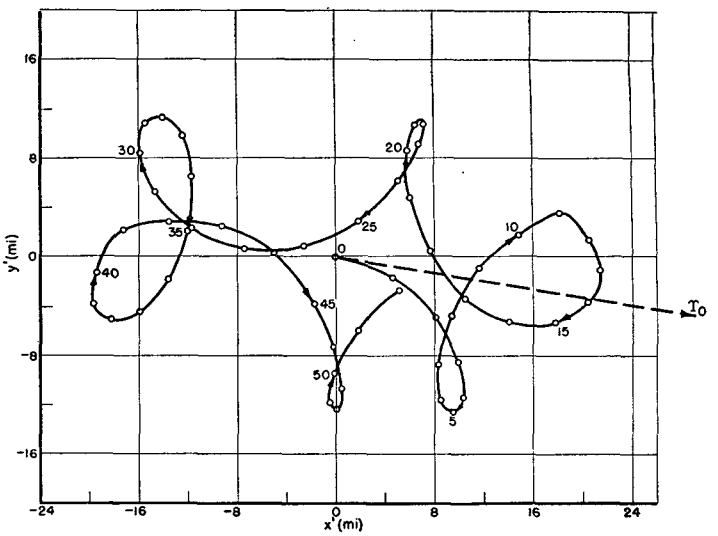

FIG. 4. Zone A_1 relative trajectory for maximum effective amplitude.

Examples of relative trajectories for typical cases in zones A_1 and A_2 will now be presented. The significant features of relative perturbed motion depend only on values of b, c, λ, and Υ_0, although the actual form of the motion depends on the variables M_x, M_y, N_x, λ, and Υ_0. Specific and likely values of these variables were taken in each case; for all cases $\Upsilon_0 = 5$ miles hr^{-1} and $\lambda = 0.4$ hr^{-1} ($\phi = 49.6°N$). The zone A_1 case has $b = +2.25$ and $c = +0.234$. In fig. 4 is shown the relative trajectory corresponding to a maximum effective amplitude. The origin of the (x', y') axes represents the position of the unperturbed parcel at any time. The relative position of the perturbed parcel is shown at intervals of one hour by circles, which are numbered at intervals of 5 hr. The solid line therefore represents the horizontal projection of the isentropic relative trajectory. The dashed line gives the orientation of the initial impulse velocity, Υ_0.

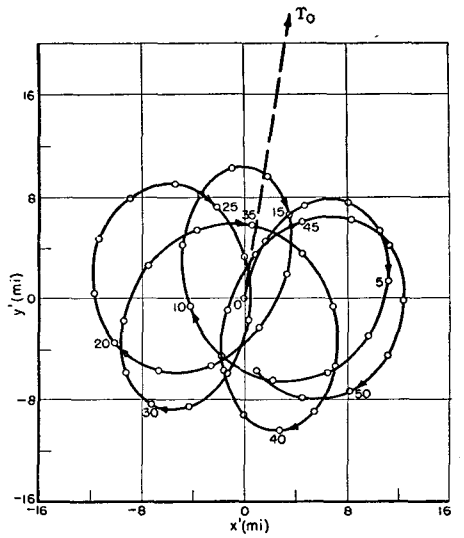

FIG. 5. Zone A_1 relative trajectory for minimum effective amplitude.

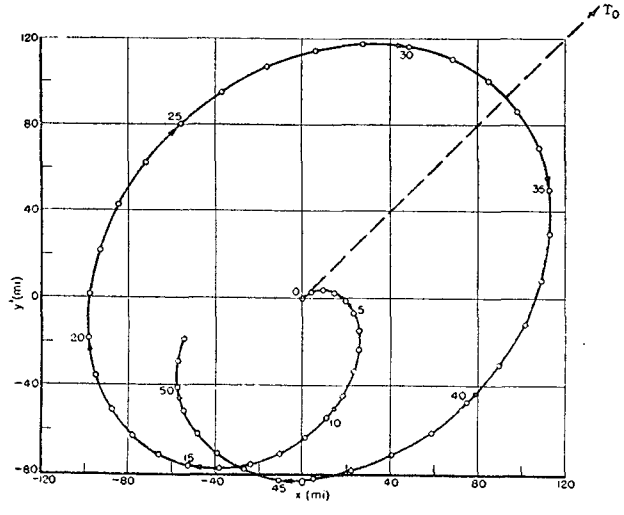

FIG. 6. Zone A_2 relative trajectory for maximum effective amplitude.

In fig. 5 is shown the relative trajectory corresponding to a minimum effective amplitude. The mean effective amplitude has the value 11.5 miles, for an initial relative perturbation velocity of 5 miles hr^{-1}. This value illustrates clearly the great stability of zone A_1 displacements.

A typical example of zone A_2 was computed with b and c values of $+0.50$ and $+0.0469$, respectively. The maximum effective amplitude trajectory is shown in fig. 6, the minimum in fig. 7. The mean effective amplitude in this case was 74 miles, considerably greater than the value of 11.5 miles for the zone A_1 example.

It may be mentioned that maximum and minimum values of $\overline{\Upsilon^2}$ are associated with maximum and minimum values of $\overline{r^2}$, respectively, as might be anticipated. In zone A_2 $\overline{\Upsilon^2} > \Upsilon_0^2$, in zone A_1 $\overline{\Upsilon^2} < \Upsilon_0^2$, corresponding to an increase or a decrease, respectively, in the random, relative kinetic energy of the perturbation.

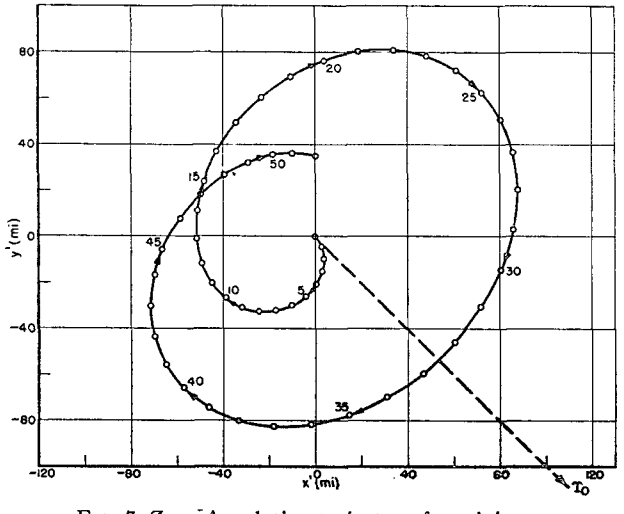

FIG. 7. Zone A_2 relative trajectory for minimum effective amplitude.

6. Perturbed motion in zone of pure imaginary frequencies

In zone C, the roots of the frequency equation are pure imaginary, corresponding to hyperbolic functions for x', y', and z'. The appropriate solutions are

$$x' = A(\cosh \alpha_1 t - \cosh \alpha_2 t) + B_1 \sinh \alpha_1 t + B_2 \sinh \alpha_2 t, \quad (36)$$

$$y' = C(\cosh \alpha_1 t - \cosh \alpha_2 t) + D_1 \sinh \alpha_1 t + D_2 \sinh \alpha_2 t. \quad (37)$$

The relations (30)–(33) for zone A apply also to zone C if ω is replaced by α and ω^2 by $-\alpha^2$. α_1 and α_2 may be obtained from fig. 2, or from (23), replacing ω^2 by $-\alpha^2$.

Zone C displacements are unstable and hence increase with time (not necessarily monotonically). Thus, a mean effective amplitude cannot be obtained and the degree of instability cannot be specified in any simple and unique manner. Even though the perturbation equations apply strictly only if t is small, it is of interest to study the nature of the solutions for relatively large values of t (of the order of 12–24 hr). The simpler asymptotic solutions thereby obtained can be used to specify, in an approximate manner, the degree of instability in zones B, C, and D.

The first result obtained is that the orientation of the relative motion approaches a fixed direction, independent of the initial impulse orientation, specified by

$$\left(\frac{y'}{x'}\right)_\infty = \left(\frac{\dot{y}'}{\dot{x}'}\right)_\infty = \left(\frac{\Upsilon_y}{\Upsilon_x}\right)_\infty = \frac{\lambda N_x + \alpha_1^2}{\lambda(\alpha_1 + M_x)} = \frac{\lambda(\alpha_1 - M_x)}{\lambda M_y - \alpha_1^2}, \quad (38)$$

where α_1 denotes the larger hyperbolic parameter. It will be shown, by examples, that this deduction applies with considerably greater rigor to zone D instability than to zone C. Fortunately, the occurrence of zone D instability in the atmosphere far exceeds that of zone C instability. Nevertheless, in zone C the relative perturbed motion *is not random*, but represents accelerated motion approaching the direction defined by (38). This direction is of considerable physical significance since it represents what may be called the "perturbation-divergence axis." Along this axis-line, which passes through the moving, unperturbed parcel, perturbed parcels are being accelerated away from the unperturbed parcel in the two opposite directions defined above. If an area of type C dynamic instability exists in the atmosphere, the area itself will experience horizontal divergence as it moves and the compensating convergence will be found beyond the area in the opposite directions specified by (38).

The mean of r^2, as a function of time, for two trajectories initially orthogonal again represents the mean for all possible trajectories. Thus, it is possible to

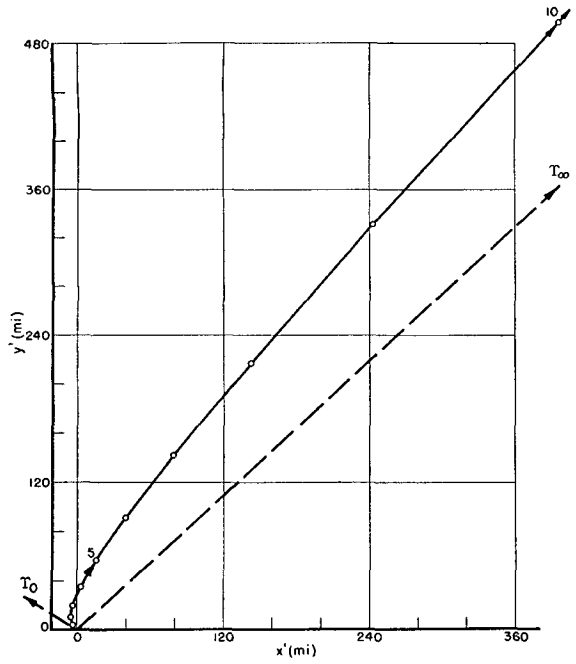

FIG. 8. Zone C relative trajectory for maximum effective amplitude.

obtain a relation for the root-mean-square relative displacement, a time-dependent function, which will be valid for large t but which will also afford a qualitative measure of the degree of instability for small t. This relation is

$$(\overline{r^2})^{\frac{1}{2}} = \left[\frac{(b-1)^2 - 4c}{2(b^2-4c)}\right]^{\frac{1}{2}} \frac{\Upsilon_0 \sinh \alpha_1 t}{\alpha_1}. \quad (39)$$

An illustrative example for zone C was computed, using the standard values of Υ_0 and λ (5 miles hr^{-1} and 0.40 hr^{-1}, respectively) and b and c values of -1.125 and $+0.234$, respectively. In fig. 8 is shown the relative trajectory corresponding to eventual maximum displacement, in fig. 9 the relative trajectory corresponding to eventual minimum displacement. In the latter case, terms in α_1 eventually disappear so that (38) does not hold in this instance. In these figures, the direction of the asymptotic perturbed motion is indicated by the dashed line labelled Υ_∞. The degree of instability can be seen to be very great in zone C.

7. Perturbed motion in zone of real and imaginary frequencies

In zone D, one ω^2 root is positive and the other negative so that the general solution contains both trigonometric and hyperbolic functions, *i.e.*,

$$x' = A(\cosh \alpha t - \cos \omega t) + B_1 \sinh \alpha t + B_2 \sin \omega t, \quad (40)$$

$$y' = C(\cosh \alpha t - \cos \omega t) + D_1 \sinh \alpha t + D_2 \sin \omega t. \quad (41)$$

Relations (30) and (31) from zone A apply to zone D if ω_1 is replaced by ω and ω_2^2 by $-\alpha^2$. Relations (32) and (33) may be used to find B_2 and D_2, using $-A$ and $-C$; B_1 and D_1 are found from them by substituting α for ω and $-\alpha^2$ for ω^2.

Again, asymptotic solutions are found to give valuable information on the degree of instability. Relations (38) and (39) apply with greater rigor to zone D, replacing α_1 by α. In most other aspects, a zone D perturbation is very similar to a zone C perturbation. Both are unstable and do not yield random accelerated motions, but instead approach a given direction with respect to the unperturbed parcel. Both, therefore, superimpose certain moving fields of perturbation-convergence and perturbation-divergence on the ambient fields.

Illustrative examples were computed for cases in zones D_1 and D_3. It will be noted that minimum displacement trajectories have no asymptotic direction;

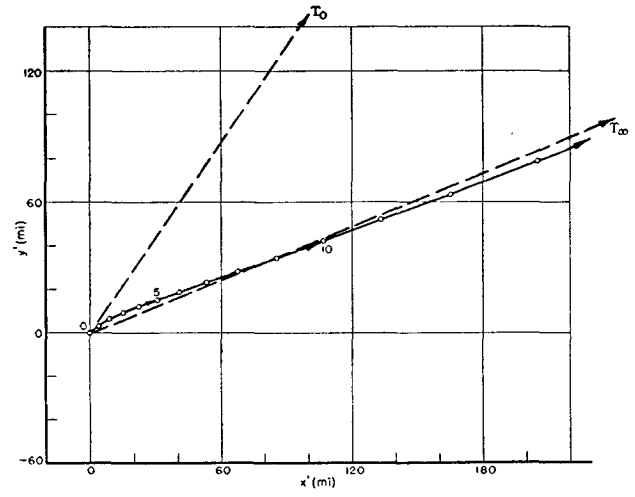

FIG. 9. Zone C relative trajectory for minimum effective amplitude.

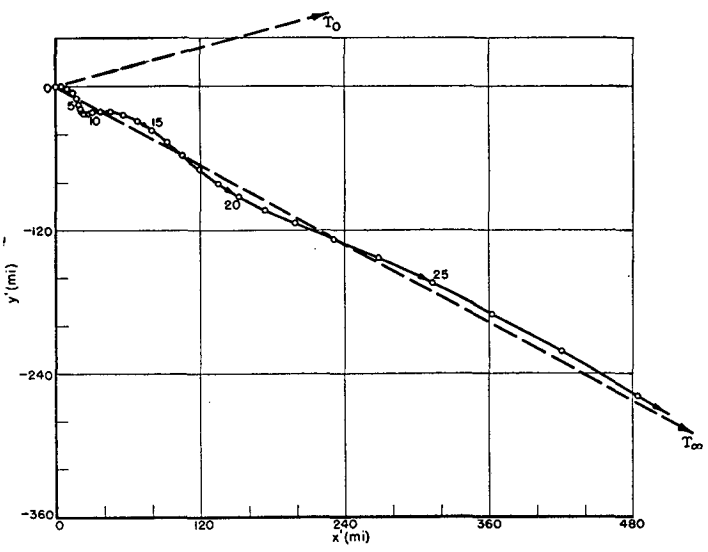

FIG. 10. Zone D_1 relative trajectory for maximum effective amplitude.

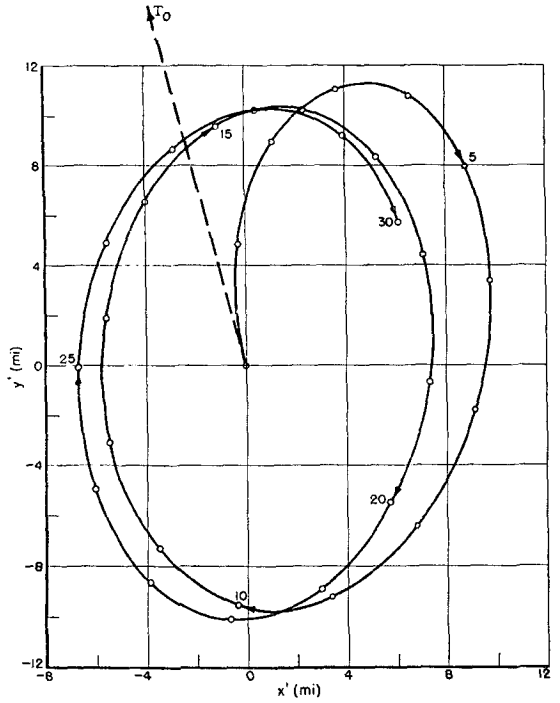

FIG. 11. Zone D_1 relative trajectory for minimum effective amplitude.

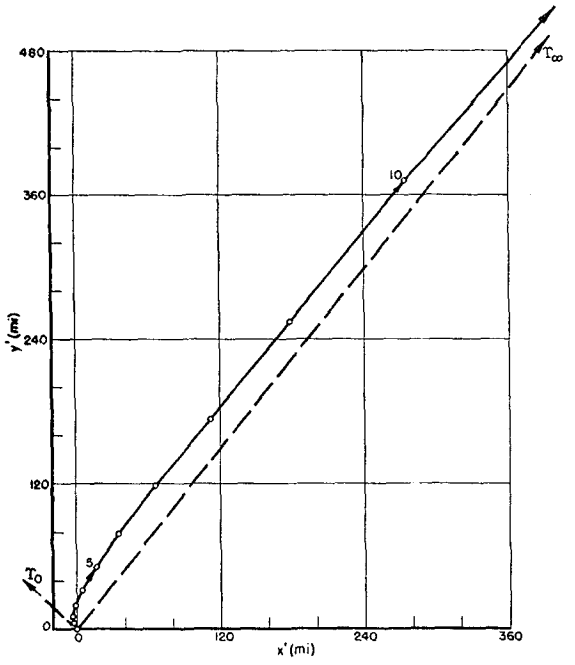

FIG. 12. Zone D_3 relative trajectory for maximum effective amplitude.

in this case, terms in α die away. The zone D_1 example has $b = +1.5$, $c = -0.203$; fig. 10 presents the eventual maximum displacement trajectory, fig. 11 the minimum. The zone D_3 example has $b = -0.625$, $c = -0.234$; fig. 12 presents the eventual maximum displacement trajectory, fig. 13 the minimum. The zone D_3 case represents a considerably greater degree of instability than the zone D_1 case, as may be seen from the diagrams.

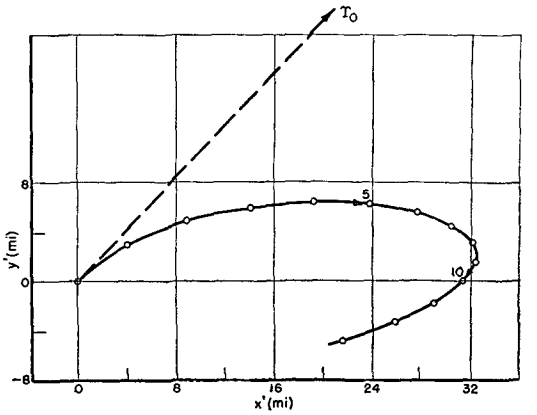

FIG. 13. Zone D_3 relative trajectory for minimum effective amplitude.

8. Perturbed motion in zone of complex frequencies

Straightforward but tedious mathematical operations reveal that the solutions appropriate to zone B are

$$x' = G_2 \cosh \alpha t \sin \omega t + G_3 \sinh \alpha t \cos \omega t + G_4 \sinh \alpha t \sin \omega t, \quad (42)$$

$$y' = H_2 \cosh \alpha t \sin \omega t + H_3 \sinh \alpha t \cos \omega t + H_4 \sinh \alpha t \sin \omega t. \quad (43)$$

α and ω are not direct roots of (23) but are found from the relations

$$(\alpha/\lambda) = (-\tfrac{1}{4}b + \tfrac{1}{2}c^{\frac{1}{2}})^{\frac{1}{2}}, \quad (44)$$

$$(\omega/\lambda) = (\tfrac{1}{4}b + \tfrac{1}{2}c^{\frac{1}{2}})^{\frac{1}{2}}. \quad (45)$$

A set of curves for fixed values of (α/λ) is entered in zone B of fig. 2; (ω/λ) is obtained from the value of (α/λ) when b is replaced by $-b$.

The relations between the constants in (42) and (43) are

$$\alpha(\lambda^2 - 4\omega^2)G_3 = -\omega\lambda(M_y + N_x)G_2 + 2\omega\lambda M_x H_2, \quad (46)$$

$$\alpha(\lambda^2 - 4\omega^2)G_4 = \lambda^2 M_x G_2 - \lambda(\alpha^2 + \omega^2 - \lambda M_y)H_2, \quad (47)$$

$$\alpha(\lambda^2 - 4\omega^2)H_3 = 2\omega\lambda M_x G_2 + \omega\lambda(M_y + N_x)H_2, \quad (48)$$

and

$$\alpha(\lambda^2 - 4\omega^2)H_4 = \lambda(\alpha^2 + \omega^2 + \lambda N_x)G_2 - \lambda^2 M_x H_2. \quad (49)$$

G_2 and H_2 may be obtained from Υ_{0_x} and Υ_{0_y} by using the relations

$$(\lambda^2 - 4\omega^2)\Upsilon_{0_x} = \omega[\lambda^2 - \lambda(M_y + N_x) - 4\omega^2]G_2 + 2\omega\lambda M_x H_2, \quad (50)$$

$$(\lambda^2 - 4\omega^2)\Upsilon_{0_y} = 2\omega\lambda M_x G_2 + \omega[\lambda^2 + \lambda(M_y + N_x) - 4\omega^2]H_2. \quad (51)$$

In the case of zone B perturbations, the mean of r^2 for two initially-orthogonal relative trajectories is no

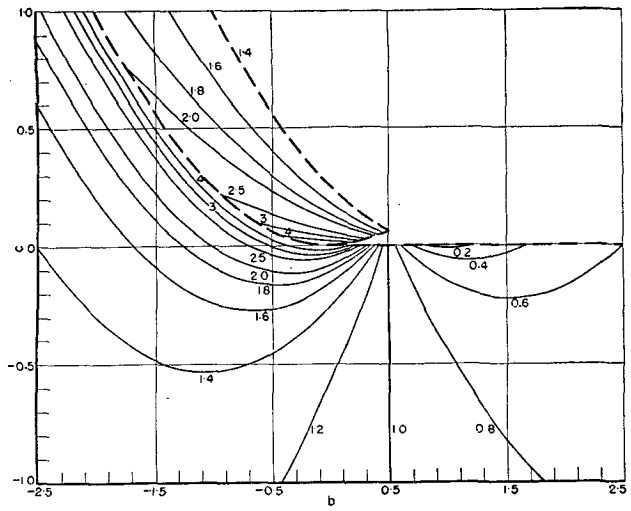

FIG. 14. Time-independent coefficient of root-mean-square amplitude.

longer independent of the set chosen. An approximate value of the time-dependent root-mean-square displacement can be obtained from the asymptotic solutions, of sufficient validity for a qualitative assessment of the degree of instability in zone B. Such an analysis reveals that there is no unique value of $(y'/x')_\infty$, but that, instead, the relative trajectory is an expanding spiral. The analysis gives the following approximate equation for the root-mean-square displacement:

$$(\overline{r^2})^{\frac{1}{2}} = [\tfrac{1}{8}c^{-1}(1-b)(1-b+2c^{\frac{1}{2}})]^{\frac{1}{2}}\alpha^{-1}\Upsilon_0 \sinh \alpha t. \quad (52)$$

This may be written as

$$(\overline{r^2})^{\frac{1}{2}} = \frac{\Upsilon_0}{2^{\frac{1}{2}}}\frac{\sinh \alpha t}{\alpha} S_B. \quad (53)$$

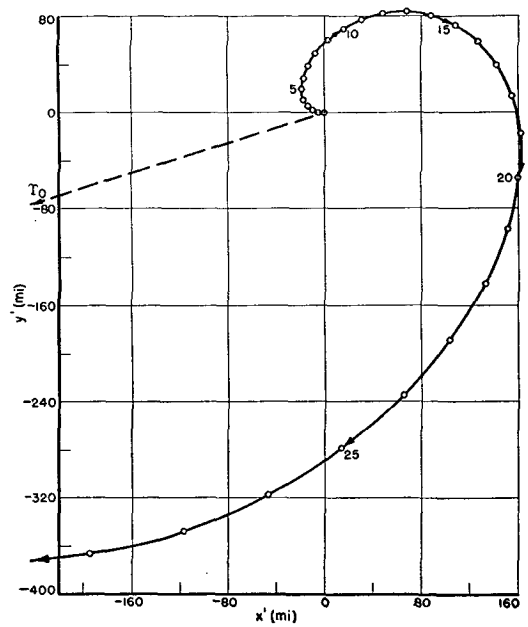

FIG. 15. Zone B_2 relative trajectory for maximum effective amplitude.

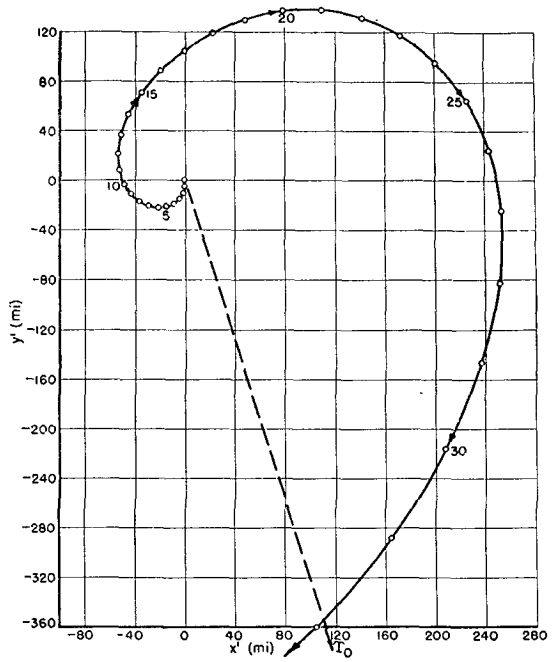

FIG. 16. Zone B_2 relative trajectory for minimum effective amplitude.

The corresponding relation for zones C and D is

$$(\overline{r^2})^{\frac{1}{2}} = \frac{\Upsilon_0}{2^{\frac{1}{2}}}\frac{\sinh \alpha t}{\alpha} S_{C,D}, \quad (54)$$

where $S_{C,D}$ can be obtained from (39). Isopleths of the S function have been entered on the (b, c) diagram of fig. 14. The S isopleths are not continuous at the $B_3 - C_3$ boundary, as opposed to the (α/λ) isopleths in fig. 2 which are continuous. The explanation is that the solutions for zones B and C are not valid for $\omega = 0$ and $\alpha_1 = \alpha_2$, respectively. In the vicinity of the boundary, the actual solutions contain terms in $\sinh \alpha t$, $t \cosh \alpha t$ and $t \sinh \alpha t$. An analysis of asymp-

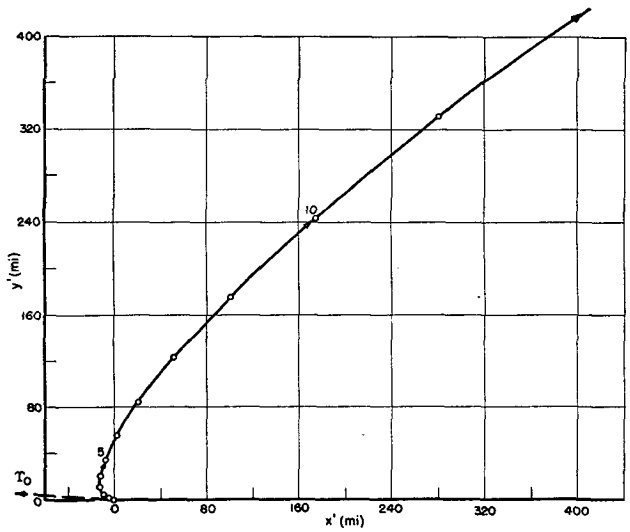

FIG. 17. Zone B_3 relative trajectory for maximum effective amplitude.

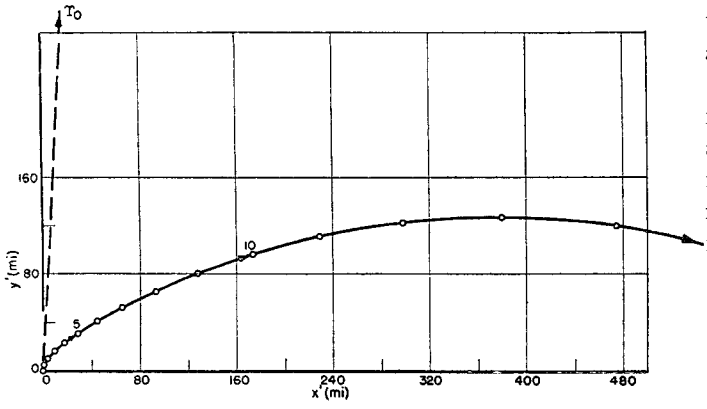

FIG. 18. Zone B_3 relative trajectory for minimum effective amplitude.

totic solutions yields the following approximate expression for the root-mean-square displacement as a function of time:

$$(\overline{r^2})^{\frac{1}{2}} = [\tfrac{1}{2}b^{-\frac{1}{2}}(2b-1)^{\frac{1}{2}}\lambda t]\alpha^{-1}\Upsilon_0 \sinh \alpha t. \quad (55)$$

Thus, the S function at the $B_3 - C_3$ boundary increases linearly with the time.

As a typical case for zone B_2, the following values are employed: $b = +0.375$, $c = +0.0781$. Fig. 15 shows the relative trajectory corresponding to the maximum average displacement, fig. 16 that for the minimum. The zone B_3 example utilizes the values $b = -0.75$, $c = +0.3594$; fig. 17 presents the maximum displacement trajectory, fig. 18 the minimum. The degree of instability is considerably greater in zone B_3 than in zone B_2, and as a result the spiral nature of the relative trajectory in the former case is evident only if the solution is extended to very large values of the relative displacement.

9. Computation of stability-criterion terms

To assess the nature of the dynamic stability or instability, it is necessary to know the quantities b and c, defined by (24), (25), and (21).

It will be recalled that the x-axis is horizontal, but otherwise arbitrary. The computation of b and c is simplified if the x-axis is chosen in the direction of the geostrophic wind at the point for which stability-criterion parameters are to be evaluated. The y-axis will thus be normal to the height contours (or isobars) and directed towards lower height (or lower pressure).

The three shears represented in (21) can readily be interpreted in terms of geostrophic streamline-patterns on isentropic charts. With the above axis convention, M_x is a measure of the streamline convergence (if positive) or divergence (if negative). M_y is a measure of the geostrophic wind shear normal to the streamlines, being positive if the speed increases to the left of the geostrophic current (anticyclonic shear) and negative if the speed decreases to the left of the current (cyclonic shear). N_x is a measure of the curvature of the streamlines, being positive for cyclonic curvature and negative for anticyclonic curvature.

Since isentropic charts are seldom available, it is necessary to compute M_x, M_y, and N_x from data appearing on constant-pressure charts and on plotted radiosonde ascents. The following equations, which can readily be derived, serve for their evaluation, two methods being indicated for M_x:

$$M_x = \left(\frac{\partial u_g}{\partial x}\right)_p + \frac{R(\partial T/\partial x)_p(\partial T/\partial y)_p}{\lambda(kT - p\,\partial T/\partial p)}, \quad (56)$$

$$M_x = -u_g\left(\frac{\partial \psi_g}{\partial y}\right)_p + \frac{R(\partial T/\partial x)_p(\partial T/\partial y)_p}{\lambda(kT - p\,\partial T/\partial p)}, \quad (57)$$

$$M_y = \left(\frac{\partial u_g}{\partial y}\right)_p + \frac{R(\partial T/\partial y)_p^2}{\lambda(kT - p\,\partial T/\partial p)}, \quad (58)$$

and

$$N_x = \frac{u_g}{r_c} - \frac{R(\partial T/\partial x)_p^2}{\lambda(kT - p\,\partial T/\partial p)}. \quad (59)$$

In these equations, $k = R/c_p$, where R is the gas constant for dry air and c_p the specific heat of dry air at constant pressure, r_c is the radius of curvature of the contour lines of a given isobaric surface (positive for cyclonic curvature), ψ_g is the angle of the geostrophic wind (measured counter-clockwise from the x-axis as positive), and $\partial T/\partial p$ represents the change of temperature with pressure in the vertical. If this rate is evaluated along a dry adiabat, kT may be evaluated as

$$kT = p\,(\partial T/\partial p)_\theta. \quad (60)$$

It is convenient to express λ, M_x, M_y, and N_x in the units hr^{-1}, in which case λ becomes

$$\lambda = 0.525 \sin \phi. \quad (61)$$

10. Dynamic instability criteria for saturated air

The derivations in the preceding sections have applied implicitly to air which was not saturated and would not become saturated by a short trajectory upslope along an isentropic surface. The instability criteria will, of course, be different for air which is saturated since it is the wet-bulb potential temperature θ_w, rather than the potential temperature θ, which will be conserved during the motions of saturated air parcels.

The formal derivation of stability criteria for saturated air is very similar to the unsaturated case; only representative equations will be presented here. The primed numbers for the equations refer to the corresponding relations for unsaturated air as previously derived. The chief problem is the evaluation of the ratio ρ_E/ρ, where ρ_E represents the density of the environment of a perturbed parcel, whose density is ρ. Define the quantity

$$\sigma = [\partial(\ln \rho)/\partial(\ln \theta_w)]_p. \quad (62)$$

Since ρ_E/ρ is approximately unity as a consequence of the small displacements being studied, (62) can be integrated in terms of θ_w , the wet-bulb potential temperature of the environment, and θ_w, the value for the perturbed parcel, considering σ to be constant. Thus,

$$\rho_E/\rho = (\theta_w/\theta_w)^{-\sigma}. \tag{3'}$$

It may be remarked that σ will be negative and will have a maximum negative value of -1. It follows from (3') that, dropping the subscript in θ_w denoting the environment,

$$\rho_E/\rho = 1 + \sigma r' \cdot \nabla(\ln \theta_w). \tag{5'}$$

The differential equations of relative motion are virtually unchanged, except that terms in $\partial(\ln \theta)$ are replaced by terms in $-\sigma\,\partial(\ln \theta_w)$. The solutions of these equations can be resolved into a component normal to wet-bulb potential temperature surfaces and a component in such surfaces. The frequency of the former component will be approximately

$$\omega = [-g\sigma\,\partial(\ln \theta_w)/\partial z]^{\frac{1}{2}}. \tag{15'}$$

The nature of the quasi-horizontal component will depend on b, c, and λ as for the unsaturated case, except that the geostrophic shears involved in the parameters are to be computed in surfaces of constant wet-bulb potential temperature. These shears can be computed using (56)–(59) if kT is replaced by $p\,(\partial T/\partial p)_{\theta_w}$, where $(\partial T/\partial p)_{\theta_w}$ refers to the temperature-pressure relation along a pseudo-adiabat. It may be noted that these considerations apply also to the case in which the perturbed parcel is saturated while the environment is unsaturated.

11. Synoptic applications

The physical significance of the release of dynamic instability and the synoptic applications of the dynamic instability criteria are discussed in a subsequent paper.[2] To stimulate thinking along the lines of the analysis in the present paper and to partially justify the conclusions drawn from such an analysis, the main features of the results of further studies are indicated here.

Briefly, it may be anticipated, from physical arguments, that the release of significant dynamic instability should be associated with a region of mass depletion, or "perturbation-divergence." Statistical studies verified this result by yielding a negative correlation between $(\overline{r^2})^{\frac{1}{2}}$ for unstable zones at 500 mb and the development tendency of surface pressure-systems. Thus, on the average, marked dynamic instability was associated with either cyclogenesis or anticyclolysis, and very weak instability and dynamic stability with cyclolysis or anticyclogenesis. It may be noted, moreover, that actual dynamic stability occurred far less frequently than dynamic instability. A majority of all cases were of the zone D type, most of which could be classified as manifesting only weak instability.

REFERENCES

Ford, L. R., 1933: *Differential equations*. New York, McGraw-Hill Book Co., p. 179.

Kleinschmidt, E., 1941: Stabilitätstheorie des geostrophischen Windfeldes. *Ann. Hydrogr. mar. Meteor.*, **69**, 305–325.

Solberg, H., 1936: Le mouvement d'inertie de l'atmosphère stable et son rôle dans la théorie des cyclones. *Procès-verbaux de l'assoc. de météor., Un. géod. géophys. Int., Edimbourg*, 66–82.

Van Mieghem, J., 1946: Contribution à l'étude de la cyclogenèse. *Inst. R. météor. Belg., Mém.*, **23**, 1–24.

——, 1947: La stabilité des mouvements atmosphériques. *Final report of Aerology Commission, O.M.I., Appendix 11*, Toronto, Doc. C. Ae. 71, 1–9.